Cryo-EM structure of the *Mycobacterium tuberculosis* cytochrome *bcc:aa*$_3$ supercomplex and a novel inhibitor targeting subunit cytochrome *c*I

Vikneswaran Mathiyazakan[1,2], Chui-Fann Wong[2], Amaravadhi Harikishore[2], Kevin Pethe[1,2,*] and Gerhard Grüber[2,*]

[1] Lee Kong Chian School of Medicine, Nanyang Technological University, 59 Nanyang Drive, Singapore 636921, Republic of Singapore, Singapore

[2] Nanyang Technological University, School of Biological Sciences, 60 Nanyang Drive, Singapore 637551, Republic of Singapore

*To whom correspondence should be addressed:

Prof. Dr. Kevin Pethe, E-mail: kevin.pethe@ntu.edu.sg

Prof. Dr. Gerhard Grüber, E-mail: ggrueber@ntu.edu.sg

Running title: Mycobacterial cytochrome oxidase, an inhibitor target

Keywords: Cytochrome *bcc:aa*$_3$ oxidase • Bioenergetics • OXPHOS • Tuberculosis • *Mycobacterium tuberculosis* • Inhibitor

Supplementary Methods

Cryo-EM grid preparation

The purified *Mtb* cyt-*bcc:aa*$_3$ was concentrated to 9 mg/ml with a 100 kDa centricon (Millipore; Burlington, WA, USA). 4 µl of sample were applied to a holey carbon grid (Quantifoil® 300 mesh R1.2/1.3 holey carbon grid; Quantifoil Micro Tools GmbH, Germany) that was glow-discharged in air for 1 min. Grids were blotted twice with the FEI Vitrobot (ThermoFisher Scientific; Waltham, MA, USA) for 3.5 s at 4 °C and 100% humidity before plunge-freezing in liquid ethane.

Data collection

Cryo-EM images of the *Mtb* cyt-*bcc:aa*$_3$ were recorded with a FEI Titan 300 kV TEM electron microscope (ThermoFisher Scientific; Waltham, MA, USA) equipped with a Gatan K2 direct electron detector (Gatan; Pleasanton, CA, USA). Data collection was performed automatically with the in-built EPU software. 4,635 super-resolution movies with 40 exposure frames were recorded at a magnification of 130,000 ×, yielding a pixel size of 0.53 Å/pixel. The camera exposure rate and total exposure were 6.6 *e*- per pixel per second and 40 *e*- per Å^2.

Image analysis

Image analysis for the *Mtb* cyt-*bcc:aa*$_3$ was performed with CryoSPARC and RELION v3.1.[1, 2] MotionCor2 was used to correct local beam-induced motion and alignment of frames with a 5 x 5 patches.[3] Defocus and astigmatism were estimated with CTFFIND4.[4] An automated particle picking was performed which resulted in 206,495 particles. The particles were binned by a factor of two and subjected to multiple rounds of 2D- and 3D classifications, producing a final dataset of 73,909 particles. Next, particles were re-extracted at full resolution and subjected to 3D non-uniform refinement. The final map was post-processed with a soft-

edge mask, yielding a resolution of 4.63 Å. The map was then transferred to RELION v3.1 to utilize the Bayesian polishing function to improve the resolution further. This resulted in a final map with a resolution of 4.52 Å which was then used for model building.

Model building and refinement

The cryo-EM structure of the hybrid *Mtb* cyt-*bcc* and *M. smegmatis* cyt-aa_3 (PDB 7E1V)[5] was rigidly fitted into the density maps using UCSF ChimeraX.[6] Model of *M.tb* cyt-*bcc:aa*3 was built from the EM maps with Coot and Phenix.[7, 8] Manual adjustments and refinements were performed using Coot and further real-space refinements were performed in Phenix.[7, 8] Multiple cycles of refinements were performed to optimize the models. The quality of the final models was evaluated with MolProbity.[7-9] Visualizations, generation of figures and/or movies were performed with UCSF ChimeraX, UCSF Chimera, and open-sourced PyMOL v2.4 (Schrödinger 2017; New York, USA).[5,10,11]

Homology modelling

The *Mycobacterium tuberculosis* (*Mtb*) QcrC model was generated using homology modelling online tool - SWISS-MODEL server. The 3D model of the *Mtb* QcrC was generated using the *M. smegmatis* cryo-EM structure (PDB ID: 6HWH, resolved at 3.4 Å) as a template. The heme groups were modelled in to the *Mtb* QcrC complex based on the *M. smegmatis* structure. The quality of the homology model was evaluated using procheck algorithm.[12,13]

Protein Preparation

The *Mtb* QcrA/C subunit assembly model was prepared by fixing the bond orders of the cofactors—porphyrin rings, heme atoms and the ligated histidine residues. The substrate (MQ9) and other heteroatoms other than Co-factors of QcrA/C molecules were removed during

the refine step of protein preparation. The refined protein was energy minimized until the heavy atoms converged to 0.3 Å r.m.s.d. using OPLS force field in protein preparation wizard and Macromodel modules in Schrödinger suite of programs. [14,15]

Ligand preparation

Enamine discovery collection of more than two million molecules was employed for virtual screening studies. Using default settings with ligand preparation and energy minimization tools, the 2D library was converted into 3D and energy minimized.

Grid preparation and docking

The mycobacterial specific α3-helix was used to define the site point for grid generation using default settings in glide. The Enamine 3D library was run through high-throughput virtual screening (HTVS) mode, the standard precision (SP) mode, and extra precision (XP) mode using default settings. The hits thus characterized were also further assessed for their fitness by docking into the experimentally determined *Mtb* QcrAC subunits of cyt-*bcc* cryo-EM structure from this study. All molecular modelling simulations were performed on a Linux workstation.

$DMNQH_2$ reaction kinetics assay

2,3-Dimethyl-1,4-naphthoquinone (DMNHQ) was purchased from Enamine, USA. 20 mM of DMNQ was prepared in 1 ml ethanol containing 6 mM HCl. The DMNQ solution was reduced with a few grains of sodium borohydride ($NaBH_4$) in an ice bath. 10 µl of 12 N HCl was used to quench the reaction. This reaction resulted in the formation of $DMNQH_2$.

Purified *Mtb* cyt-*bcc:aa*$_3$ was resuspended in 500 µl reaction buffer (20 mM MOPS, pH 7.4, 100 mM NaCl, 0.01% DDM) to a final concentration of 65 nM. $DMNQH_2$ was serially diluted from a starting concentration of 200 µM and used to initiate respiration respectively. This

initiated respiration within the supercomplex, was monitored by a Clark-type oxygen electrode (Oxytherm^{+}, Hansatech, Pentney, United Kingdom). The oxygen consumption curve was plotted using GraphPad Prime 8.0 software.[16]

cyt*Mycc*I inhibitor kinetics assay

2,3-Dimethyl-1,4-naphthoquinone and cyt*Mycc*I were purchased from Enamine, USA. 20 mM of DMNQ was prepared in 1 ml ethanol containing 6 mM HCl. The DMNQ solution was reduced with a few grains of sodium borohydride ($NaBH_4$) in an ice bath. 10 µl of 12 N HCl was used to quench the reaction. This reaction resulted in the formation of $DMNQH_2$.

Purified *Mtb* cyt-*bcc:aa*$_3$ was resuspended in 500 µl reaction buffer (20 mM MOPS, pH 7.4, 100 mM NaCl, 0.01% DDM) to a final concentration of 65 nM. cyt*Mycc*I was serially diluted from a starting concentration of 250 µM and incubated with the resuspended supercomplex respectively at 4 ^{o}C for 1 hour. 5 µl of $DMNQH_2$ was added to the mixture to yield a final concentration of 100 µM. This initiated respiration within the supercomplex, was monitored by a Clark-type oxygen electrode (Oxytherm^{+}, Hansatech). The oxygen consumption curve was plotted using GraphPad Prime 8.0 software.[16]

References

1. Punjani A, Rubinstein JL, Fleet DJ, Brubaker MA. 2017. cryoSPARC: algorithms for rapid unsupervised cryo-EM structure determination. Nature Methods 14:290-296.
2. Zivanov J, Nakane T, Forsberg BO, Kimanius D, Hagen WJH, Lindahl E, Scheres SHW. 2018. New tools for automated high-resolution cryo-EM structure determination in RELION-3. eLife 7:e42166.

3. Zheng SQ, Palovcak E, Armache JP, Verba KA, Cheng Y, Agard DA. 2017. MotionCor2: anisotropic correction of beam-induced motion for improved cryo-electron microscopy. Nature Methods 14:331-332.
4. Rohou A, Grigorieff N. 2015. CTFFIND4: Fast and accurate defocus estimation from electron micrographs. Journal of Structural Biology 192:216-21.
5. Zhou S, Wang W, Zhou X, Zhang Y, Lai Y, Tang Y, Xu J, Li D, Lin J, Yang X, Ran T, Chen H, Guddat LW, Wang Q, Gao Y, Rao Z, Gong H. 2021. Structure of Mycobacterium tuberculosis cytochrome bcc in complex with Q203 and TB47, two anti-TB drug candidates. eLife 10:e69418.
6. Goddard TD, Huang CC, Meng EC, Pettersen EF, Couch GS, Morris JH, Ferrin TE. 2018. UCSF ChimeraX: Meeting modern challenges in visualization and analysis. Protein Science 27:14-25.
7. Afonine PV, Poon BK, Read RJ, Sobolev OV, Terwilliger TC, Urzhumtsev A, Adams PD. 2018. Real-space refinement in PHENIX for cryo-EM and crystallography. Acta crystallographica. Section D, biological crystallography 74:531-544.
8. Emsley P, Lohkamp B, Scott WG, Cowtan K. 2010. Features and development of Coot. Acta crystallographica. Section D, biological crystallography 66:486-501.
9. Williams CJ, Headd JJ, Moriarty NW, Prisant MG, Videau LL, Deis LN, Verma V, Keedy DA, Hintze BJ, Chen VB, Jain S, Lewis SM, Arendall WB, 3rd, Snoeyink J, Adams PD, Lovell SC, Richardson JS, Richardson DC. 2018. MolProbity: More and better reference data for improved all-atom structure validation. Protein Science 27:293-315.
10. Pettersen EF, Goddard TD, Huang CC, Couch GS, Greenblatt DM, Meng EC, Ferrin TE. 2004. UCSF Chimera—A visualization system for exploratory research and analysis. Journal of Computational Chemistry 25:1605-1612.

11. Schrödinger Release 2019-2 (2019) Maestro, Force Fields, MacroModel, prime, protein preparation wizard, Ligprep, ConfGen, Phase, QikProp, Glide. Schrödinger, LLC, New York, NY
12. Laskowski RA, Rullmann JAC, MacArthur MW, Kaptein R, Thornton JM: AQUA and PROCHECK-NMR: programs for checking the quality of protein structures solved by NMR. Journal of biomolecular NMR 1996, 8(4):477-486.
13. Sasisekharan RGRC: Stereochemistry of polypeptide chain configurations J Mol Biol 79599. Ramachandran GN, Ramakrishnan C, and Sasisekharan (1963). Stereochemistry of polypeptide chain configurations. Journal of molecular biology 1963, 7:95-99.
14. Madhavi Sastry G, Adzhigirey M, Day T, Annabhimoju R, Sherman W: Protein and ligand preparation: parameters, protocols, and influence on virtual screening enrichments. Journal of computer-aided molecular design 2013, 27(3):221-234.
15. Schrödinger Release 2019-2 (2019) Maestro, Force Fields, MacroModel, prime, protein preparation wizard, Ligprep, ConfGen, Phase, QikProp, Glide. Schrödinger, LLC, New York, NY
16. Motulsky, H.; Christopoulos, A. Fitting Models to Biological Data Using Linear and Nonlinear Regression: A Practical Guide to Curve Fitting; GraphPad Software Inc.: San Diego, CA, USA, 2003; Available online: www.graphpad.com (accessed on 21 September 2021).

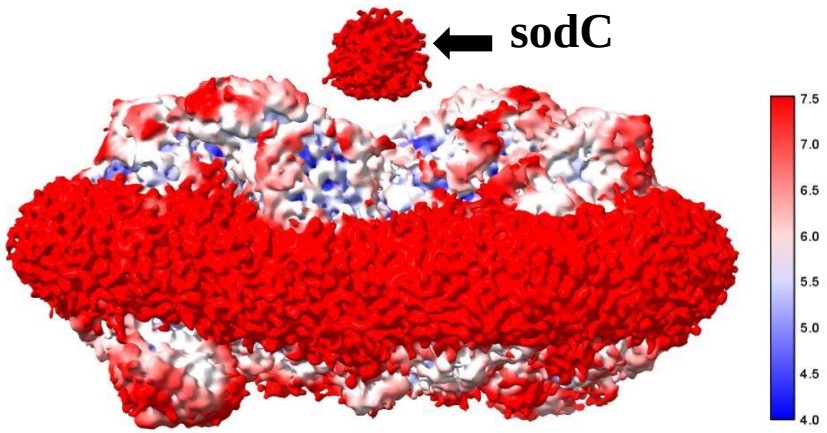

Supplementary Figure S1. Local resolution estimation of *Mtb* sodC. The dark red regions indicate a 7.5 Å resolution while the dark blue region denotes a 4 Å resolution. sodC was shown to have a high resolution of 7.5 Å.

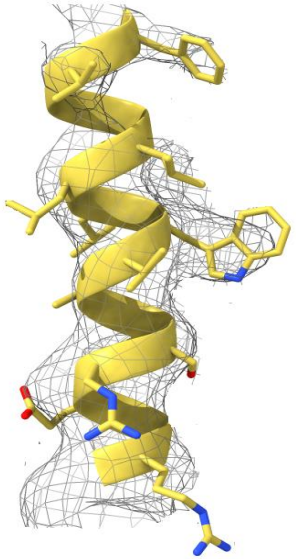

QcrA$_{91\text{-}106}$

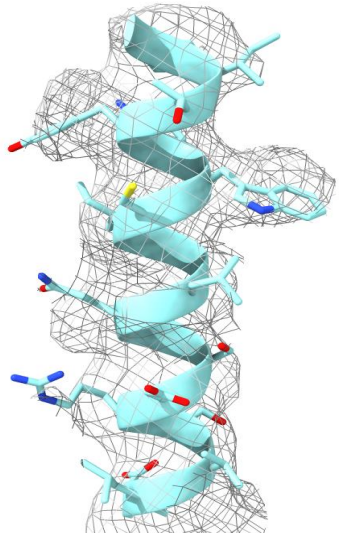

QcrB $_{429\text{-}447}$

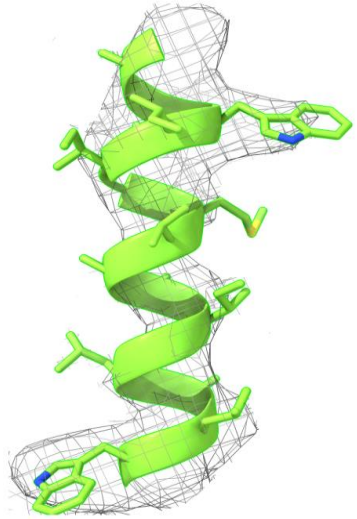

QcrC $_{260\text{-}275}$

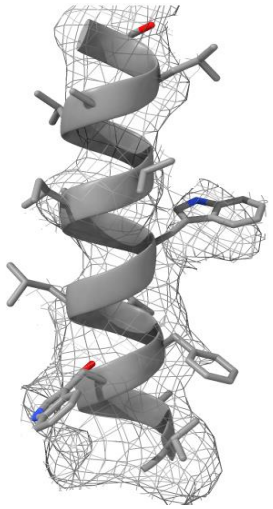

CtaC $_{57\text{-}73}$

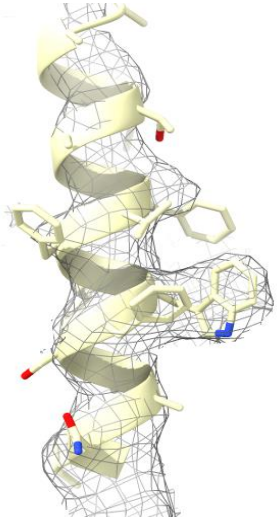

CtaD $_{121\text{-}140}$

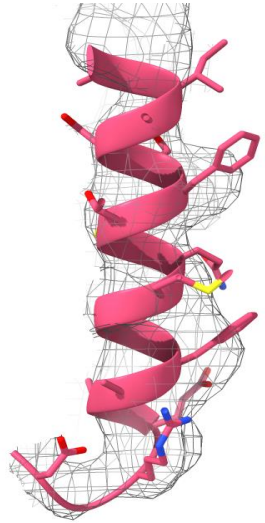

CtaE $_{77\text{-}95}$

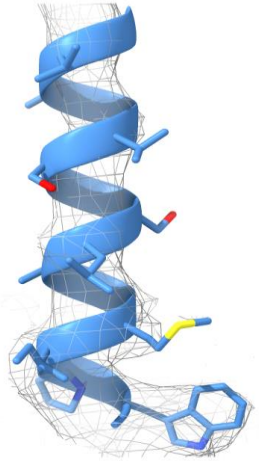

CtaF $_{91\text{-}105}$

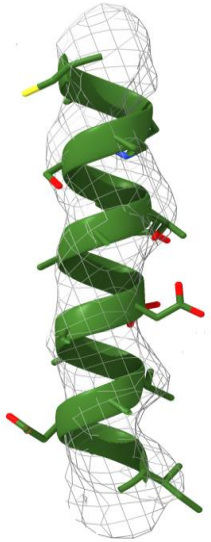

CtaI $_{45\text{-}62}$

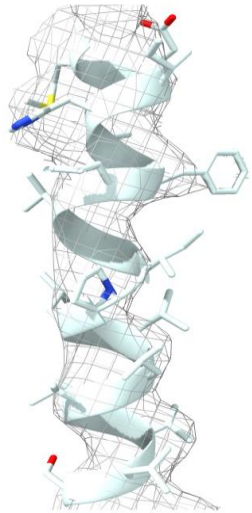

CtaJ $_{4\text{-}22}$

Supplementary Figure S2. Cryo-EM map and model fit analysis of individual subunit backbone and side chain residues of the *Mtb* cyt-*bcc:aa*$_3$ structure.

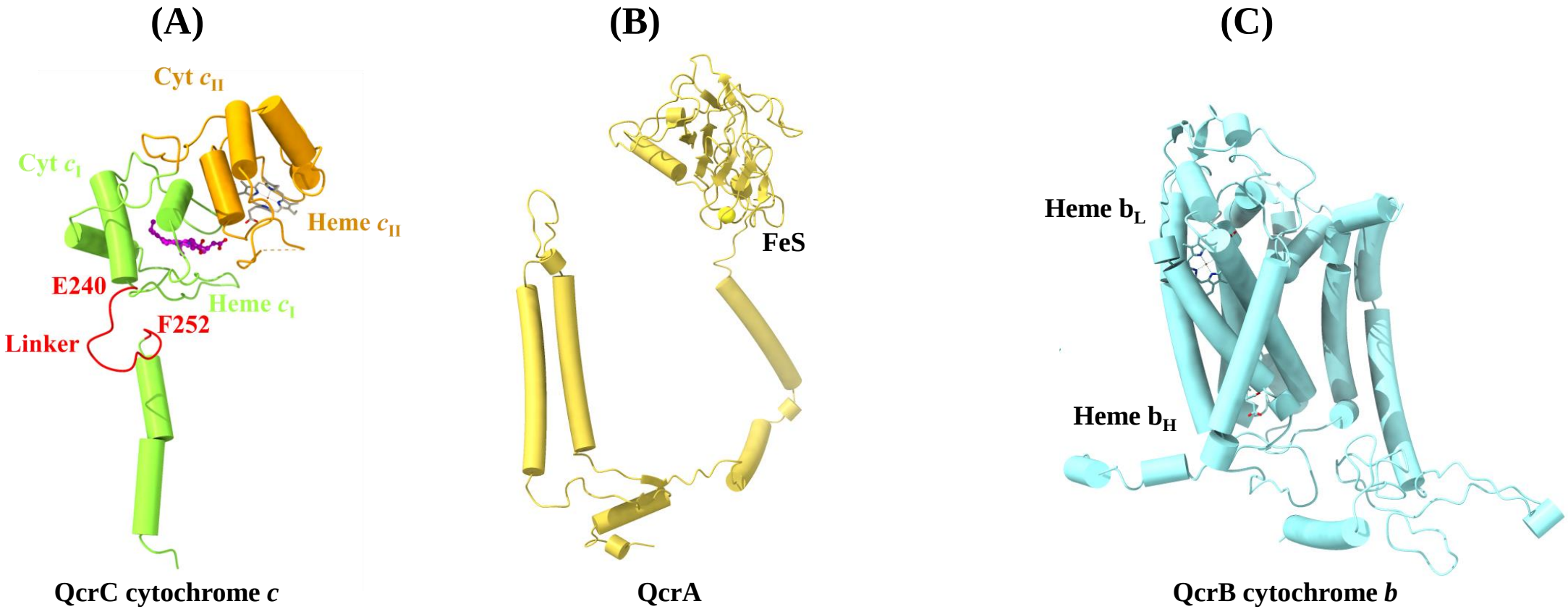

Supplementary Figure S2A. Structures of the resolved *Mtb* cyt-*bcc* subunits. The cyt-*bcc* complex consists of subunits QcrC (A), QcrA (B) and QcrB (C).

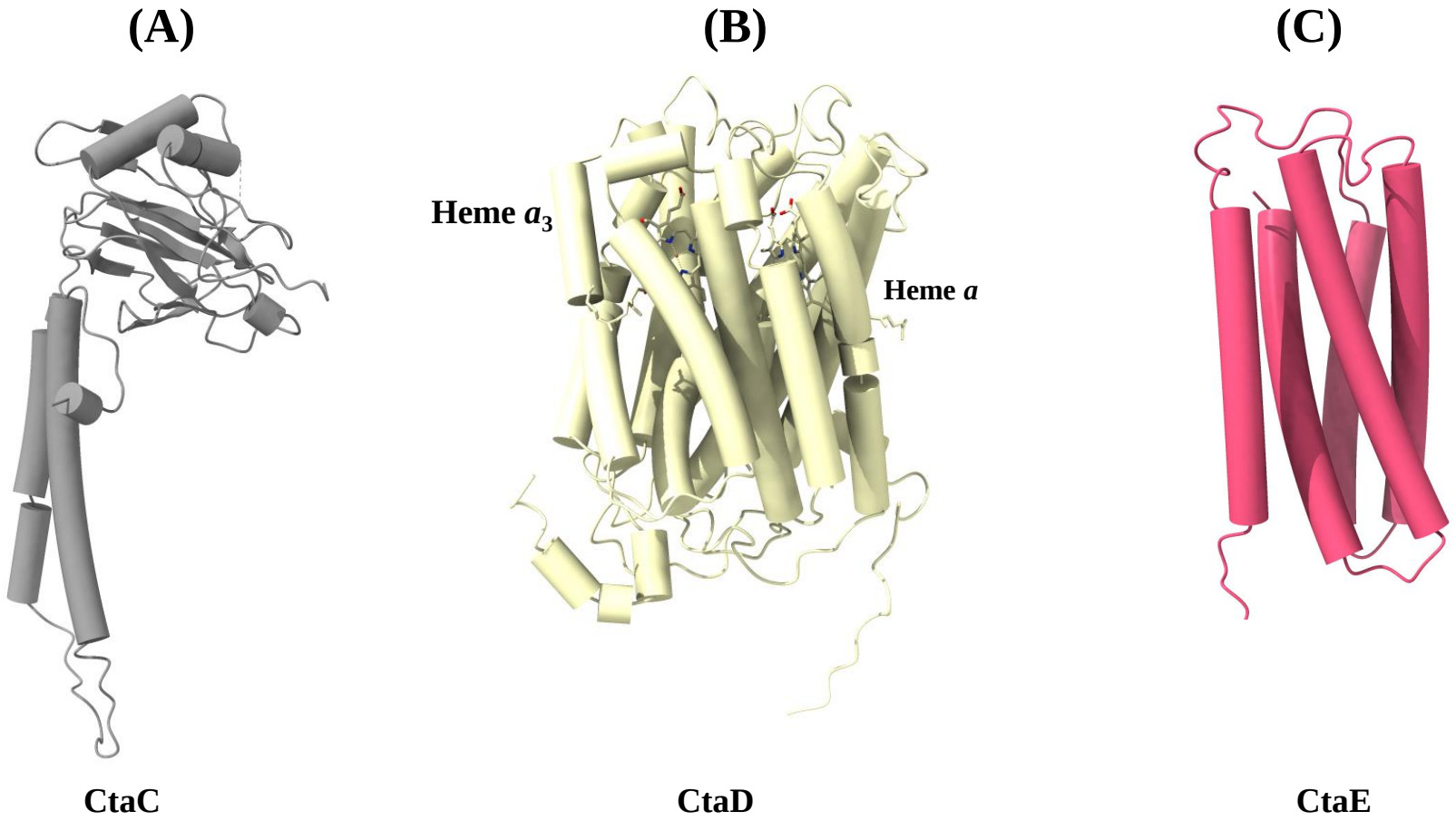

Supplementary Figure S2B. Derived structures of the *Mtb* cyt-aa_3 subunits CtaC (A), CtaD (B) and CtaE (C).

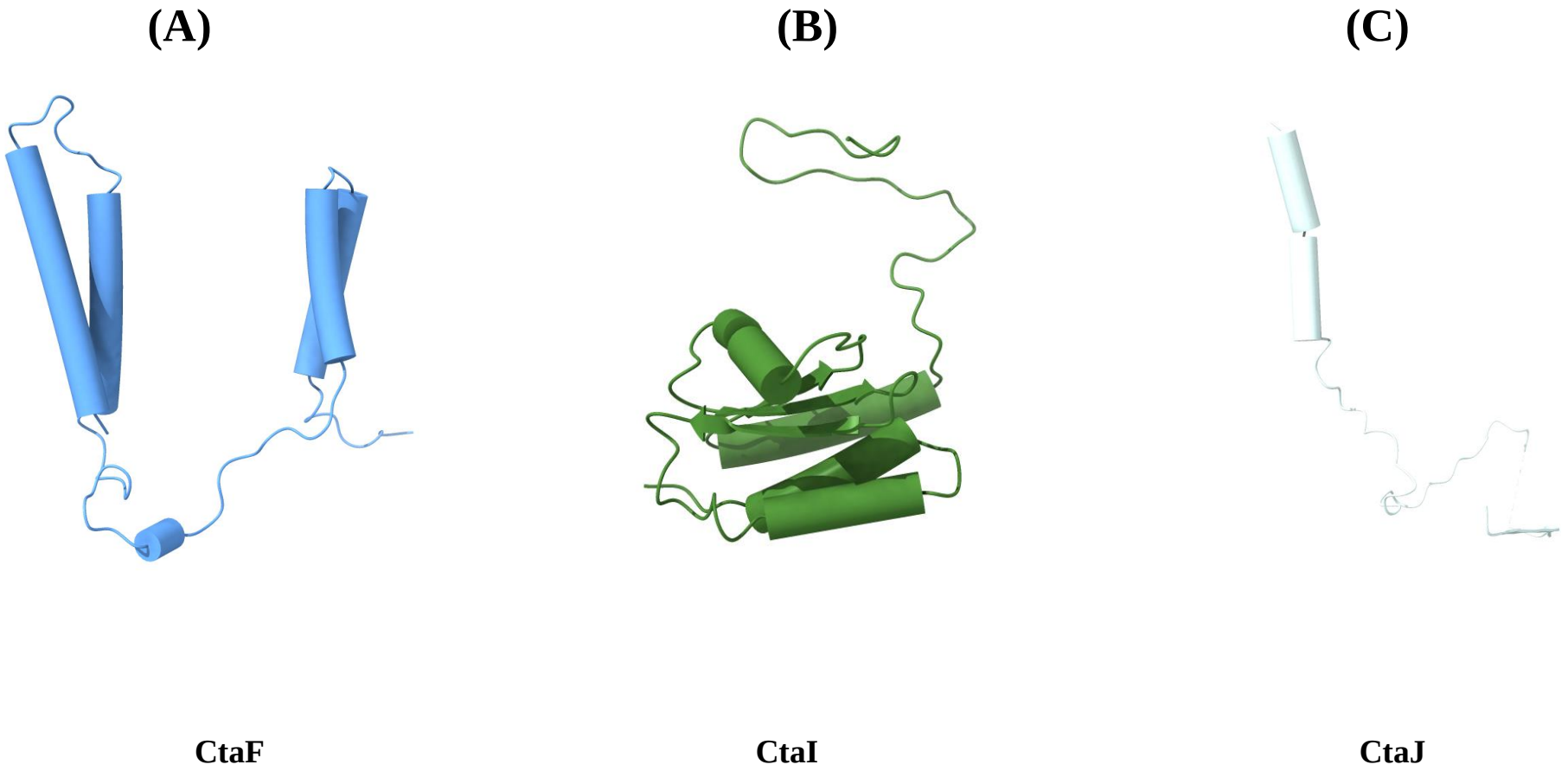

Supplementary Figure S2C. Structures of the *Mtb* cyt-aa_3 assembly subunits CtaF (A), CtaI (B) and CtaJ C).

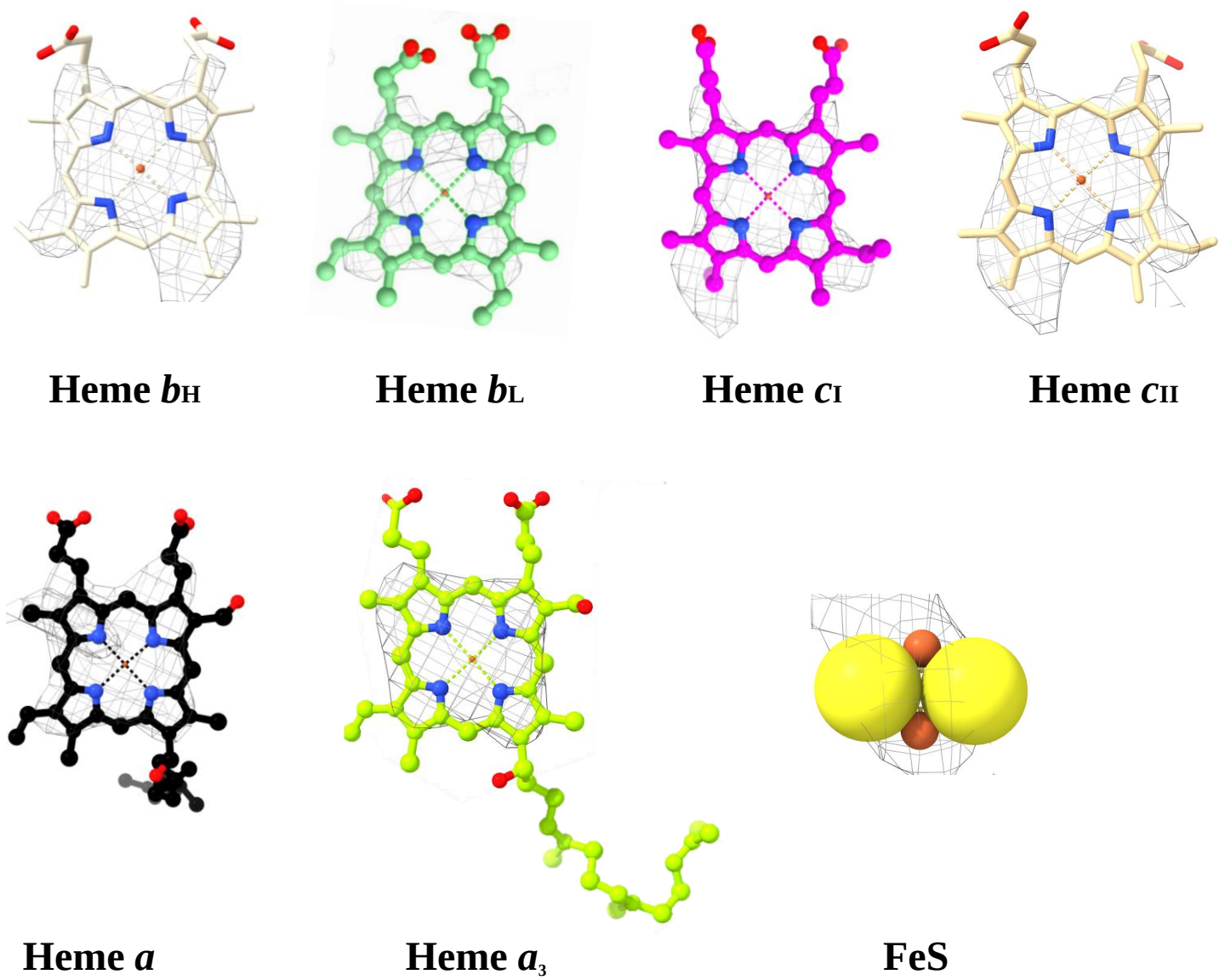

Supplementary Figure 3. Cryo-EM map and model fit analysis of reaction centers in resolved *Mtb* cyt-*bcc:aa*$_3$ structure.

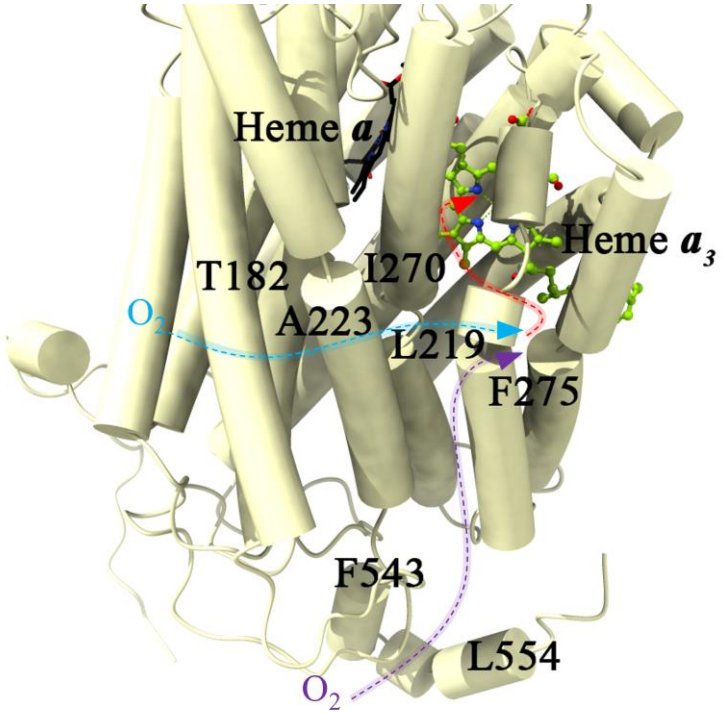

Supplementary Figure 4. Proposed oxygen diffusion pathway in the *Mtb* cyt-*bcc:aa*$_3$. The diffusion of oxygen to heme a_3 has a Y-shaped channel, including two entry points. The first entrance is flanked by A223 and L219 (*blue*) and the second one is flanked by F543 and L554 (*purple*). The two channels converge at F275 to continue to I270 via the *red* channel and finally reach heme a_3.

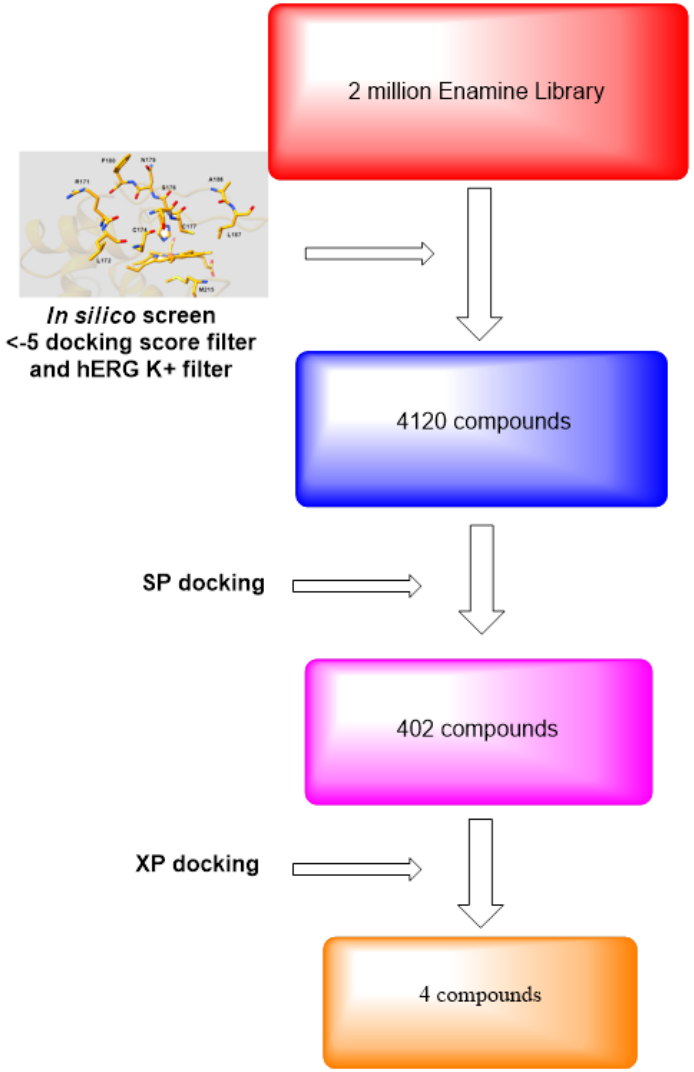

Supplementary Figure 5. A virtual screening campaign to identify novel chemical entities.

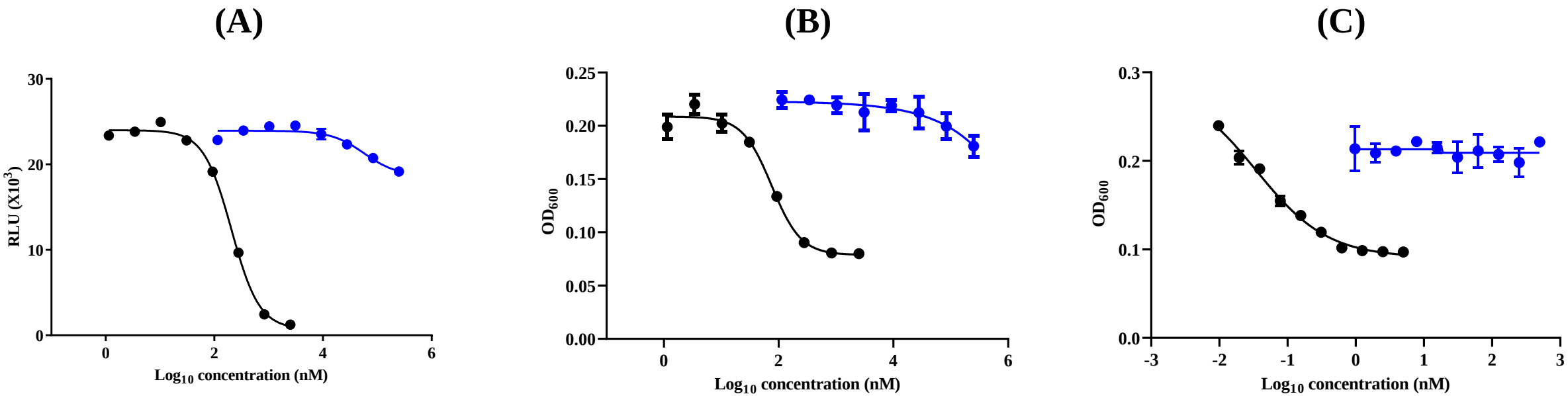

Supplementary Figure 6. Activity of cyt*Mycc*1 whole cell assays (A) Effect of cyt*Mycc*1 (*blue circles*) on the intracellular ATP levels in *M. bovis* BCG wildtype (WT) strain. The bacteria were treated with a dose-range of cyt*Mycc*1 and bedaquiline (BDQ; *black circles*) for 15 hours before quantification of intracellular ATP levels. All experiments were performed in triplicate and repeated at least once. The data are expressed as the mean ± SDs of triplicates for each condition. (B) Growth inhibitory activity of cyt*Mycc*1 (*blue circles*) against WT *M. bovis* BCG. The bacteria were treated with a dose-range of cyt*Mycc*1 and BDQ (*black circles*) for 5 days before growth inhibitory potency of the compounds were recorded. All experiments were performed in triplicate and repeated at least once. The data are expressed as the mean ± SDs of triplicates for each condition. (C) Growth inhibitory activity of cyt*Mycc*1 (*blue circles*) against WT *M. smegmatis*. The bacteria were treated with a dose-range of cyt*Mycc*1 and BDQ (*black circles*) for 48 hours before growth inhibitory potency of the compounds were recorded. All experiments were performed in triplicates and repeated at least once. The data are expressed as the mean ± SDs of triplicates for each condition.

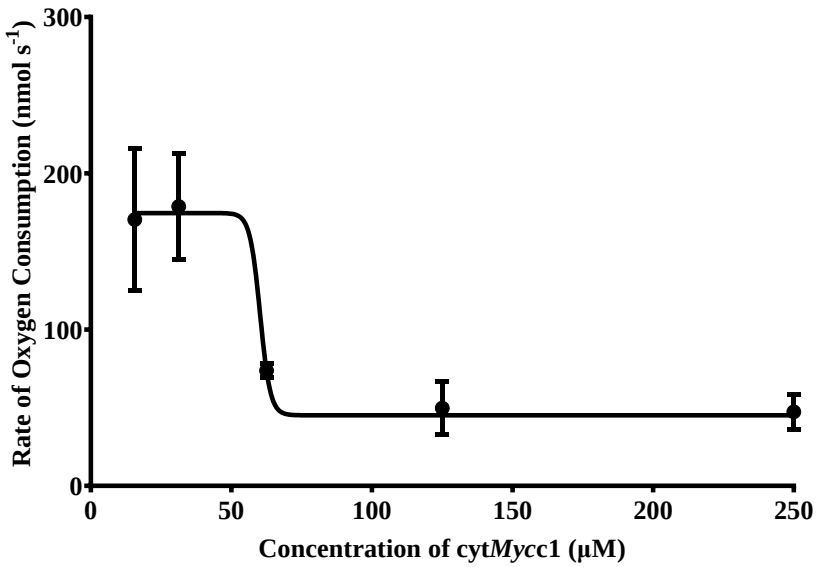

Supplementary Figure 7. Reaction kinetics of cyt*Mycc*1 against *Mtb cyt-bcc:aa*$_3$ in an oxygen consumption assay. The recombinant protein was incubated with a dose-range of cyt*Mycc*1 (*black circles*) for 1 hour before determining the effect on oxygen reduction in the presence of 100 µM of 2,3-dimethyl[1,4]naphthohydroquinone. A dose-response relationship was observed with 250 µM of cyt*Mycc*1 causing 4-fold reduction in rate of oxygen consumption after subtracting background activity.

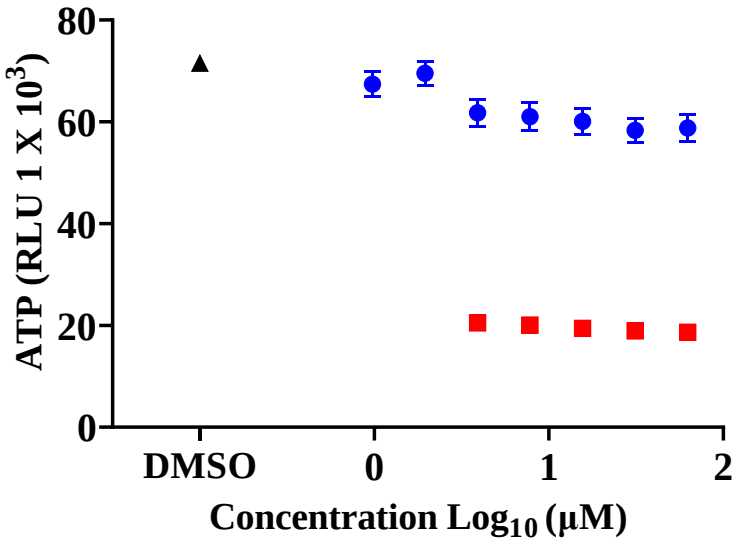

Supplementary Figure 8. Activity of cyt*Mycc*1 in *E. coli* wildtype inverted membrane vesicles (IMVs). The IMVs were treated with a dose-range of cyt*Mycc*1 (*blue circles*) and potassium cyanide (KCN; *red squares*) for 50 min before quantification of ATP levels. All experiments were performed in triplicate.